Structures of NADH and CH_3-H_4Folate Complexes of *Escherichia coli* Methylenetetrahydrofolate Reductase Reveal a Spartan Strategy for a Ping-Pong Reaction[†,‡]

Robert Pejchal, Ryan Sargeant,[§] and Martha L. Ludwig*

Department of Biological Chemistry and Biophysics Research Division, The University of Michigan, Ann Arbor, Michigan 48109-1055

Received March 23, 2005; Revised Manuscript Received June 13, 2005

ABSTRACT: Methylenetetrahydrofolate reductases (MTHFRs; EC 1.7.99.5) catalyze the NAD(P)H-dependent reduction of 5,10-methylenetetrahydrofolate (CH_2-H_4folate) to 5-methyltetrahydrofolate (CH_3-H_4folate) using flavin adenine dinucleotide (FAD) as a cofactor. The initial X-ray structure of *Escherichia coli* MTHFR revealed that this 33-kDa polypeptide is a $(\beta\alpha)_8$ barrel that aggregates to form an unusual tetramer with only 2-fold symmetry. Structures of reduced enzyme complexed with NADH and of oxidized Glu28Gln enzyme complexed with CH_3-H_4folate have now been determined at resolutions of 1.95 and 1.85 Å, respectively. The NADH complex reveals a rare mode of dinucleotide binding; NADH adopts a hairpin conformation and is sandwiched between a conserved phenylalanine, Phe223, and the isoalloxazine ring of FAD. The nicotinamide of the bound pyridine nucleotide is stacked against the *si* face of the flavin ring with C4 adjoining the N5 of FAD, implying that this structure models a complex that is competent for hydride transfer. In the complex with CH_3-H_4folate, the pterin ring is also stacked against FAD in an orientation that is favorable for hydride transfer. Thus, the binding sites for the two substrates overlap, as expected for many enzymes that catalyze ping-pong reactions, and several invariant residues interact with both folate and pyridine nucleotide substrates. Comparisons of liganded and substrate-free structures reveal multiple conformations for the loops $\beta2-\alpha2$ (L2), $\beta3-\alpha3$ (L3), and $\beta4-\alpha4$ (L4) and suggest that motions of these loops facilitate the ping-pong reaction. In particular, the L4 loop adopts a "closed" conformation that allows Asp120 to hydrogen bond to the pterin ring in the folate complex but must move to an "open" conformation to allow NADH to bind.

Methylenetetrahydrofolate reductases (MTHFRs)[1] catalyze the reaction that provides one-carbon units for the conversion of homocysteine to methionine (Scheme 1). The MTHFR reaction is the sole route to methyltetrahydrofolate, the donor for the remethylation of homocysteine that is catalyzed by cobalamin-dependent and cobalamin-independent methionine synthases (MetH and MetE, respectively). MTHFRs catalyze the transfer of a hydride ion from NAD(P)H to methylenetetrahydrofolate (CH_2-H_4folate) using bound flavin adenine dinucleotide (FAD) as an intermediate hydride acceptor and donor. MTHFR is the only enzyme known to catalyze the direct exchange of a hydride between folate and FAD. In ribothymidine synthase, reduced flavin is believed to react with the nucleotide rather than with methylenetetrahydrofolate (*1*).

Scheme 1: Reactions Catalyzed by MTHFR[a]

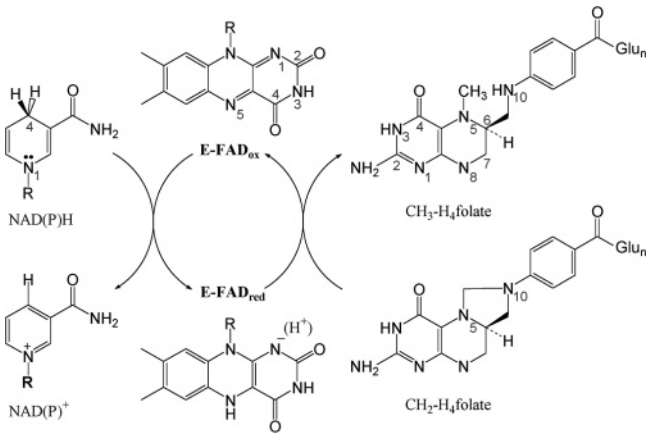

[a] Formulas show the numbering for the isoalloxazine and tetrahydrofolate ring systems. The conversion of methylenetetrahydrofolate to methyltetrahydrofolate is presumed to proceed via an intermediate iminium cation formed by the opening of the imidazolidine ring (*16*).

[†] Financial support was received from the National Institutes of Health (GM16429 to M.L.L. and GM08720 to R.P.).

[‡] The atomic coordinates and structure factors (codes 1ZP3, 1ZP4, 1ZPT, and 1ZRQ) have been deposited in the Protein Data Bank, Research Collaboratory for Structural Bioinformatics, Rutgers University, New Brunswick, NJ.

* To whom correspondence should be addressed. E-mail: mlludwig@umich.edu. Fax: (734) 764-3323. Telephone: (734) 647-2736.

[§] Present address: Chemistry Department, Brigham Young University, Idaho, Rexburg, ID 83460-0500.

[1] Abbreviations: MTHFR, methylenetetrahydrofolate reductase; APS, Advanced Photon Source; MetE, cobalamin-independent methionine synthase; MetH, cobalamin-dependent methionine synthase; FAD, flavin adenine dinucleotide; CH_3-H_4folate, *N*5-methyl-5,6,7,8-tetrahydrofolate; CH_2-H_4folate, *N*5,*N*10-methylene-5,6,7,8-tetrahydrofolate; NAD(P)H, nicotinamide adenine dinucleotide (phosphate); *S*-AdoMet, *S*-adenosylmethionine; TIM, triose phosphate isomerase.

10.1021/bi050533q CCC: $30.25
Published on Web 08/02/2005

The enzymes from pig liver and from *Homo sapiens* are homodimers of 70−77-kDa chains, each consisting of a catalytic domain and regulatory regions that mediate allosteric responses to *S*-adenosylmethionine (*S*-AdoMet) (*2*, *3*). These mammalian enzymes are specific for NADPH (*4*). Bacteria express simpler MTHFR enzymes in which the catalytic domain constitutes the entire sequence. *Escherichia coli* MTHFR (EC 1.7.99.5), the best characterized of these enzymes, utilizes NADH rather than NADPH for reduction of CH_2-H_4folate (*5*). It is a homotetramer (*5*, *6*) of 33-kDa chains, each 296 residues in length (*7*).

Steady-state and transient kinetic studies of the mammalian and bacterial enzymes, from the laboratories of Buchanan et al. (*8*, *9*), Kutzbach and Stokstad (*4*), and Matthews and co-workers (*5*, *10*−*12*) have established that the reaction proceeds as shown in Scheme 1. The data from these studies are all consistent with a ping-pong reaction mechanism. In both the mammalian and bacterial enzymes, each of the half-reactions contributes to k_{cat} (*11*, *13*). Substrate inhibition, which is often observed in enzymes that display ping-pong kinetics, is especially pronounced in MTHFR, where NAD(P)H binds tightly to the reduced enzyme and CH_2-H_4-folate binds tightly to the oxidized species (*5*, *11*). Both NAD(P)H and methylenetetrahydrofolate react at the *si* face of the flavin ring (*14*) and are thus expected to occupy overlapping binding sites.

The crystal structure of substrate-free MTHFR from *E. coli* revealed that the catalytic domain is a $(\beta\alpha)_8$ barrel and was the first example of a triose phosphate isomerase (TIM) barrel enzyme that binds FAD. Subsequently, FAD-dependent proline dehydrogenase has also been shown to be a $(\beta\alpha)_8$ barrel (*15*). In MTHFR, the *re* face of the isoalloxazine ring is completely buried; as expected, the *si* face is open and accessible to solvent and substrates (Figure 1A).

Unlike most pyridine nucleotide-dependent enzymes, MTHFR does not display fingerprint sequences that are typical for pyridine nucleotide binding, nor does it incorporate a pyridine nucleotide-binding subdomain. To determine how pyridine nucleotides bind and interact with *E. coli* MTHFR, we have now analyzed the structure of a complex of the reduced wild-type enzyme with NADH. Folate binding has been examined in a complex of CH_3-H_4folate with the *E. coli* Glu28Gln enzyme, a mutant protein that does not catalyze the reversible half-reaction between reduced FAD and CH_2-H_4folate (*16*) (Scheme 1). We have also analyzed a structure of substrate-free MTHFR at 1.85 Å resolution, using data from crystals equilibrated at pH 7.4. A comparison with the initial structure determined at pH 6.1 (*17*) and with the NADH and CH_3-H_4folate complexes has revealed pH-dependent conformational equilibria that are coupled to substrate binding.

The structures reported in this paper show how the enzyme adapts to react with two chemically and structurally distinct substrates that occupy overlapping binding sites. In particular, the loop bearing the active-site residue Asp120 alternates between "open" and "closed" conformations to provide differential recognition of NADH and folate, while Phe223 adopts alternate positions to bind either NADH or folate.

MATERIALS AND METHODS

Histidine-tagged wild-type and Glu28Gln MTHFR were overexpressed and purified as previously described (*5*). The

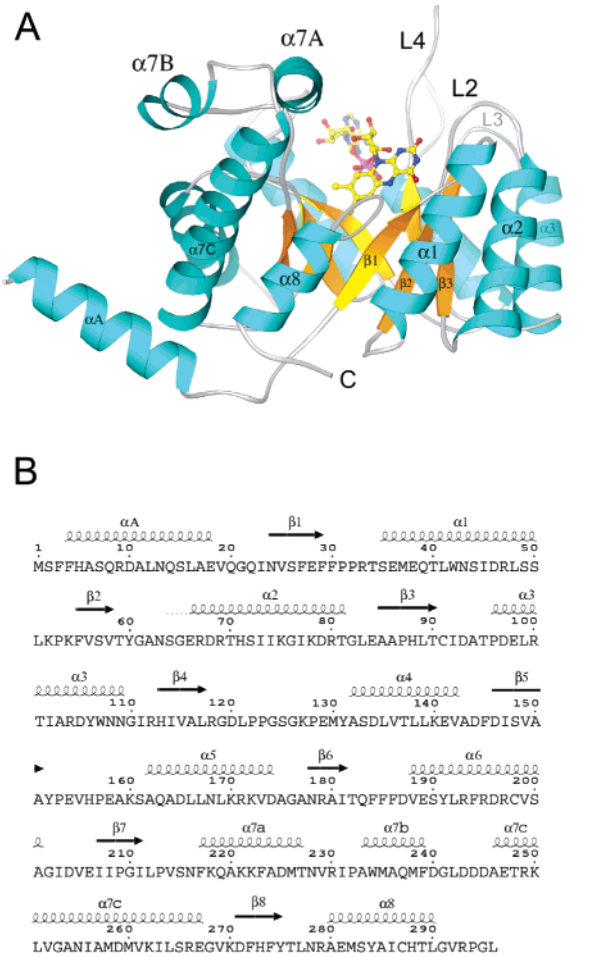

FIGURE 1: (A) Ribbon drawing of the fold of *E. coli* MTHFR. The view is toward the *si* face of the flavin and along the binding groove that is occupied by folate side chains. The MTHFR monomer is an $(\beta\alpha)_8$ barrel with three extra-barrel helices. The N-terminal αA helix makes contacts at the dimer interface, while helix 7A defines one side of the folate-binding groove. Loops that connect β strands with their following helices extend above the barrel in this view and are numbered to match the strands from which they emanate; e.g., L2 connects β2 with α2. (B) Assignments of the secondary structures and other features of the MTHFR fold. The length of the β2−α2 connector (L2) depends upon pH and substrate binding (see the text).

enzyme was stored at −80 °C at a concentration of 16.5 mg/mL (500 μM in monomer) in 50 mM KP_i at pH 7.2 with 10% glycerol and 0.3 mM EDTA. Before use, excess FAD was added to thawed aliquots of the holoenzyme to yield a final concentration of 200 μM free FAD and the solution was spun at 10 000 rpm for 10 min to remove any precipitate. Crystals were obtained by the hanging drop vapor-diffusion method in combination with microseeding. For seeding, 2 μL of enzyme stock solution was mixed with 2 μL of crystallization solution (14% PEG 4000, 225 mM Li_2SO_4, 100 mM sodium cacodylate at pH 6.0, and 5% EtOH) and microseeds from a diluted fresh seed stock were introduced with a cat whisker. Initial crystals for seed production were obtained by cocrystallization with NAD^+ at pH 5.5. Assembled drops were held over 1 mL of reservoir solution and maintained in the dark at 22 °C. Yellow monoclinic crystals appeared overnight and grew to the final size within 1 week. Crystals of wild-type histidine-tagged MTHFR belong to space group *C*2 (a = 103.24 Å, b = 127.79 Å, c = 97.70 Å, and β = 121.55°) and contain three chains in

Table 1: Data and Refinement Statistics

parameter/crystal	E_{ox}^{WT} (pH 7.4)	E_{red}^{WT}·NADH (pH 7.25)	E_{red}^{WT}·NADH (pH 6.0)	$E_{ox}^{Glu28Gln}$·MTHF (pH 7.4)
cell constants	$a = 103.24$ Å, $b = 127.79$ Å, $c = 97.70$ Å, $\beta = 121.55°$	$a = 103.61$ Å, $b = 127.74$ Å, $c = 97.83$ Å, $\beta = 121.73°$	$a = 102.19$ Å, $b = 128.16$ Å, $c = 96.86$ Å, $\beta = 120.94°$	$a = 103.59$ Å, $b = 127.81$ Å, $c = 97.95$ Å, $\beta = 121.88°$
resolution (Å)	20−1.85	20−1.95	20−2.20	20−1.85
completeness (%)[a,b]	99.3 (97.6)	97.9 (96.4)	99.8 (99.9)	99.4 (99.7)
R_{sym}[a,b,c]	0.047 (0.433)	0.038 (0.312)	0.065 (0.274)	0.060 (0.347)
$I/\sigma I$[a,b]	24.8 (3.0)	24.0 (4.2)	12.0 (3.0)	14.41 (3.79)
R_{cryst}/R_{free}[d,e]	0.216/0.238	0.219/0.245	0.217/0.254	0.219/0.238
correlation coefficient[f]	0.933	0.927	0.911	0.934

[a] Statistics calculated using DENZO and SCALEPACK (*18*). [b] Statistics in highest resolution shell enclosed in parentheses. [c] $R_{sym} = \sum|I_{obs} - I_{avg}|/\sum I_{obs}$. [d] $R_{cryst} = \sum||F_{obs}| - |F_{calcd}||/\sum|F_{obs}|$, where F_{obs} and F_{calcd} are the observed and calculated structure factor amplitudes, respectively. [e] R_{free} was calculated using random test sets of 5−10% of the reflections. [f] Calculated using the CCP4 program SFCHECK (*28*): $(\langle F_{obs}F_{calcd}\rangle - \langle F_{obs}\rangle\langle F_{calcd}\rangle)/[(\langle F^2_{obs}\rangle - \langle F_{obs}\rangle^2)(\langle F^2_{calcd}\rangle - \langle F_{calcd}\rangle^2)]^{1/2}$.

the asymmetric unit (Table 1). Cell dimensions for the substrate complexes are given in Table 1.

Preparation of E_{ox} at pH 7.4. Crystals of oxidized histidine-tagged MTHFR were titrated to pH 7.4 by a three-step serial transfer method. Crystals were transferred from mother liquor to pH 6.5 holding solution (15% PEG 4000, 225 mM Li_2SO_4, 100 mM sodium cacodylate at pH 6.5, and 5% EtOH) and soaked for 30 min. Subsequently, crystals were moved to cacodylate-buffered holding solutions of pH 7.0 and 7.4 and held in each solution for 30 min. The cryoprotectant, methylpentanediol (MPD), was introduced by 5 min soaks in pH 7.4 holding solution with an addition of 5 and 10% MPD.

Preparation of E_{red}−NADH at pH 7.25. Preparation of the reduced enzyme−NADH complex was undertaken after equilibrated with NAD^+ and AAD (3-aminopyridine dinucleotide) failed to reveal difference electron density corresponding to bound ligands. Crystals were titrated to pH 7.4 (see above) and transferred to holding solutions containing 5 and 10% meso-erythritol to effect cryoprotection. Transfer to cryoprotecting solution that was 80 mM in NADH (final pH 7.25) initiated reduction; this very high concentration of NADH was required to ensure rapid and complete reduction. The progress of reduction was monitored by observing the transition of the crystal from yellow to colorless. Crystals achieved full reduction in 1−2 min and were flash-cooled under liquid nitrogen and stored for several days prior to data collection. All buffers were sparged with argon prior to use. Assignment of the ligand as NADH rather than NAD^+ is considered in the Results.

Preparation of E_{red}−NADH at pH 6.0. Preparation of the reduced enzyme−NADH complex at acidic pH used the same methods as for the pH 7.25 complex (see above), except that the crystals were held at pH 6.0 throughout.

Preparation of $E^{(Glu28Gln)}_{ox}$−CH_3-H_4folate. Crystals of the oxidized Glu28Gln−CH_3-H_4folate complex were obtained by modifying the protocol for preparation of the NADH complex to include 10.0 mM CH_3-H_4folate (Eprova) and 20 mM sodium ascorbate. The final pH of the cryosolution was 7.4. Cocrystallization with CH_3-H_4folate did not lead to noticeable differences from the structure obtained by soaking the product into preformed crystals.

Data Collection and Structure Refinement. Data for the crystal of oxidized histidine-tagged MTHFR were collected with an R-AXIS IV imaging plate detector at 140 K using CuKα radiation from a Rigaku RUH3 rotating anode source. Images were collected with a 1° rotation range and a crystal−detector distance of 125 mm. Intensities for both reduced pyridine nucleotide complexes were measured under identical conditions. Some reoxidation of the reduced complexes was apparent at the end of data collection. Data for the Glu28Gln·CH_3-H_4folate complex were collected at the DND-CAT 5-IDB beamline at the Advanced Photon Source (APS) at Argonne, IL.

Data collection and refinement statistics are presented in Table 1. Intensities were integrated and scaled using DENZO and SCALEPACK (*18*) for data collected on the R-AXIS IV imaging plate or XDS (*19*) for data collected on the MAR 225 mm CCD at APS. Scaled intensities were converted to amplitudes with the CCP4 program TRUNCATE (*20*). For oxidized MTHFR, the CCP4 program MOLREP (*21*) was used for molecular replacement, employing a search model derived from the crystal structure of the histidine-tagged Glu28Gln mutant of MTHFR (Guenther, B., unpublished results). All three of the chains constituting the asymmetric unit (*17*) were included in the initial searches. The model derived from the refinement of the structure of oxidized MTHFR at pH 7.4 (this work) was in turn used to solve the NADH and CH_3-H_4folate complexes by molecular replacement with EPMR (*22*). For the substrate-free and CH_3-H_4folate structures, initial rigid-body refinement of individual chains was performed in CNS version 1.1 (*23*). For the reduced pyridine nucleotide complex, rigid-body adjustment and several rounds of conjugate-gradient least-squares minimization, *B*-factor refinement, and automated water picking were initially performed in SHELX (*24*). Subsequent refinement and rebuilding of all models was carried out with CNS version 1.1 and Xfit (XtalView version 4.0) (*25*), respectively. Rounds of refinement in CNS included simulated annealing in torsional space, coordinate minimization, and restrained individual *B*-factor adjustment with maximum-likelihood targets. Data/parameter ratios were 2.9, 2.7, 1.9, and 3.2 for the oxidized substrate-free model, NADH complex at pH 7.25, NADH complex at pH 6.0, and CH_3-H_4folate complex, respectively, when individual *B* values were refined. NCS restraints were not applied because of several differences among the chains that are described in the Results. Manual rebuilding included minor adjustment of side-chain and backbone conformations as well as *de novo* modeling of the N-terminal helix (αA) using Xfit. The initial strongest solvent peaks in the reduced pyridine nucleotide and CH_3-H_4folate complexes were identified by automated

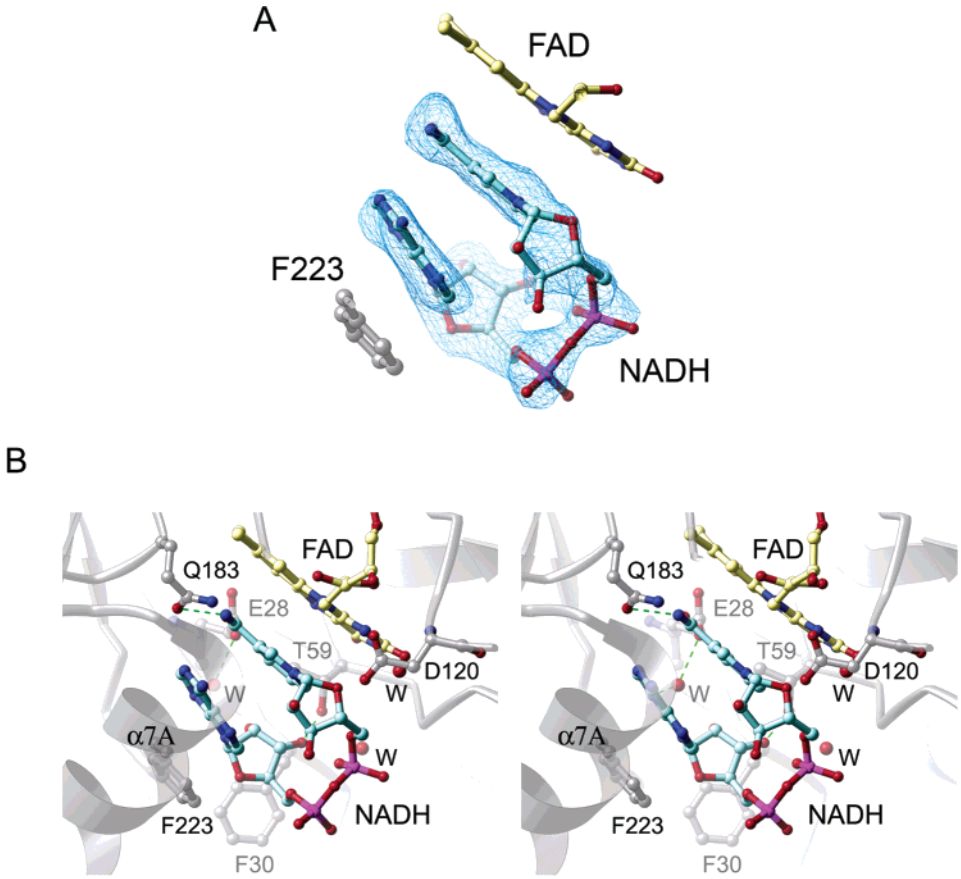

FIGURE 2: (A) Electron density corresponding to NADH in the B chain of the reduced NADH complex. The ($|F_o| - |F_c|$) map computed after annealing and refinement of a model omitting the pyridine nucleotide is contoured at 2.5σ. (B) Stereoview of the active site of reduced MTHFR with bound NADH. The pyridine nucleotide adopts a highly folded conformation and is sandwiched between the flavin ring and Phe223. The observed geometry is favorable for hydride transfer of the *pro-S* hydrogen, with FAD N5−NADH C4 separated by 3.45 Å. Hydrogen bonds between NADH and Gln183, Thr59, and the solvent are indicated with green dashed lines.

water picking in Xfit (*25*). Additional solvents were added at peaks of positive difference density with sensible chemical environments. All solvent sites were inspected, and their positions and *B* values were refined with CNS (*23*).

Clear difference densities for the pyridine nucleotide and folate ligands appeared after initial rounds of refinement of their respective complexes. NADH and CH_3-H_4folate were fit to the observed difference densities and refined with CNS using parameter and topology restraints generated with the PRO-DRG server (*26*). The *B* factors for all atoms of the three NADH molecules were first set to the value of the Wilson B for the dataset, and group occupancy refinement was undertaken for each ligand. Partial occupancies were then set at 0.85, and the individual *B* factors for NADH atoms were refined. CH_3-H_4folate sites were assumed to be fully occupied on the basis of the low group *B* factors for this ligand. In all of the structures, the average *B* factors for the A chain are much larger than for the B and C chains and the C chain displays conformational variations that are attributed to effects of crystal contacts (see the Results). Our analyses and conclusions about ligand interactions are therefore drawn principally from chain B, which exhibits small *B* factors and is free of crystal-packing artifacts.

The quality of the final models and their agreement with X-ray data were assessed with the CCP4 programs PROCHECK (*27*) and SFCHECK (*28*). The only disallowed conformation is found at Val155, which displays the same backbone arrangement in all structures. The N termini of chains A and B are visible beginning at residue 3, but the density for the C chain begins at residue 22 in all of the models. Residues 123−128 are disordered in all three chains.

RESULTS

The structure of the substrate-free enzyme is depicted in Figure 1A in an orientation that displays the open *si* face of the flavin ring where substrates bind. Secondary structure assignments are given in Figure 1B. Structures of the NADH and CH_3-H_4folate complexes, illustrated in Figures 2 and 3, define the substrate conformations and the substrate−protein interactions that are responsible for binding and specificity. In the NADH complex, the nicotinamide stacks against the *si* face of the isoalloxazine ring; residues in strands β1, β2, loop L5, and helix α7a form the remainder of the binding site for pyridine nucleotides (Figure 2B). In the CH_3-H_4folate complex (Figure 3), the pterin ring also stacks against the flavin, but the PABA moiety and glutamate tail of the folate occupy unique positions that do not overlap the subsite for the AMP of NADH.

NADH Conformation and Interactions. There are several reasons to conclude that the ligand visualized in the active site is NADH rather than NAD^+. The half-reaction of NADH with oxidized flavin proceeds in the crystal, but we expect that, in the presence of very high concentrations of NADH, the NAD^+ product will be replaced to yield the doubly reduced E_{red}−NADH species. This expectation is supported

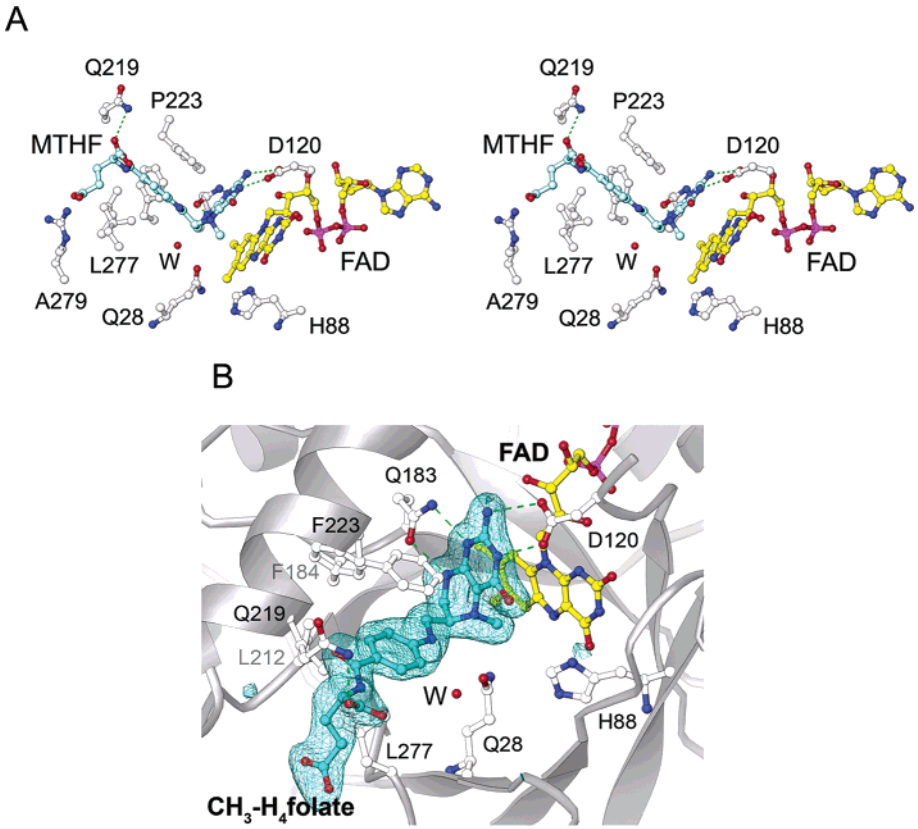

FIGURE 3: (A) Stereoview showing bound CH_3-H_4folate, FAD, and selected active-site residues. CH_3-H_4folate is shown in light green; FAD is shown in yellow; and protein residues are shown in silver. The pterin ring adjoins the flavin isoalloxazine ring and is oriented by Asp120 and Gln183. The PABA ring is surrounded by a hydrophobic box (formed by Phe223, Phe184, Leu212, and Leu277) that is open at its front face. The α-carboxyl group is bound by Gln219, while the γ-carboxyl group is bound by Arg279. Gln28 (Glu28 in wild-type MTHFR) coordinates a water that is close to the folate N10. (B) Conformation of bound CH_3-H_4folate and its interactions with the protein. The electron density is from an omit map (3σ) computed after simulated annealing and refinement. CH_3-H_4folate is shown in cyan; FAD is shown in yellow; and protein residues are shown in silver. Asp120 and Gln183 form bidentate interactions with the pterin ring.

by transient kinetic studies of the reductive half-reaction in solution (*11*), which indicate rapid dissociation of the oxidized product. Further, NADH acts a substrate inhibitor ($K_i \sim 10\ \mu$M), presumably by forming by E_{red}−NADH (*16*).

In the structures with NADH bound, the nucleotide adopts a tightly folded conformation with the adenine and nicotinamide rings in van der Waals contact (Figure 2A). This hairpin conformation of the bound pyridine nucleotide is achieved by unusual rotations about backbone oxygen−phosphorus bonds, particularly by the torsions at P_A-O3 and pyridine nucleotide-O5′ of the dinucleotide (*29*, *30*). Within the hairpin, the adenine and nicotinamide rings both adopt the favorable *anti* conformation with respect to the ribose moieties.

The pyridine nucleotide is wedged between the side chain of Phe223 and the isoalloxazine ring of FAD to make a 4-layer sandwich, with the N5 of FAD 3.5 Å from the C4 of NADH. The *pro-S* hydrogen of NADH is presented for hydride transfer, consistent with the known stereochemistry for the reaction catalyzed by the pig liver enzyme (*13*). Reduction of the flavin upon addition of NADH to crystals of oxidized MTHFR confirms that the observed geometry is favorable for hydride transfer (*31*, *32*). This is the second example of a tightly folded pyridine nucleotide in a complex that is competent for reaction. The first reported example was in flavin reductase PheA2 (*33*), which also catalyzes hydride transfer between pyridine nucleotide and flavin (see the Discussion).

Four residues, Gln183, Thr59, Glu28, and Phe223, play important roles in NADH binding and orientation (Figure 2B). Gln183 hydrogen bonds to the carboxamide side chain of the nicotinamide. In the NADH complex at pH 7.25, the carboxamide group is skewed in a way that suggests interactions with both Gln183 and Glu28. The hydroxyl of Thr59 forms a hydrogen bond with the 3′-hydroxyl of the adenine ribose. Glu28 coordinates a firmly bound water molecule that hydrogen bonds to N3 of adenine. This solvent is also close to the 2′-hydroxyl of the adenine ribose. Phe223 helps to support the folded binding mode of NADH by stacking against the adenine ring, forming one outer layer of the hydrophobic sandwich. The sandwich packing constrains the pyridine nucleotide hairpin in the direction perpendicular to the stacked rings, while the hydrogen-bonding interactions control the rotation and translation of the nucleotide within the stack.

At pH 7.25, the pyrophosphate moiety of NADH is in a polar environment with solvent molecules intervening between the phosphates and residues Glu28 and Thr59. At pH 6.0, rotation of the dinucleotide hairpin brings the pyrophosphate closer to the residues that line the "bottom" of the active-site pocket. This motion is accompanied by expulsion of the bridging water at Thr59 that appears to stabilize the NADH complex at pH 7.25. As a result of this reorientation of the bound pyridine nucleotide, some of the protein−pyridine nucleotide interactions are different in the structures determined at pH 6.0 and 7.25. Rotation of the NADH

Table 2: Conformations of L2 and L4 Loops

loop/structure	E_{ox}^{WT} (pH 6.1)[a]	E_{ox}^{WT} (pH 7.4)	E_{red}^{WT}·NADH (pH 6.0)	E_{red}^{WT}·NADH (pH 7.25)[a]	$E_{ox}^{Glu28Gln}$·MTHF (pH 7.4)
L4 (Asp120)	closed[b]	open	open	open	closed
L2 (Ala62)	open	closed	open	closed	closed

[a] Previously reported structure (*17*). [b] See the text for the description of "open" and "closed" forms.

hairpin repositions the nicotinamide carboxamide group, which forms an exclusive bidentate interaction with Gln183 at pH 6.0. The two orientations of bound NADH are compared in a figure that is included in the Supporting Information.

At the resolutions of the current structures, the X-ray data cannot unambiguously determine the orientation of the carboxamide group of the nicotinamide. We have assigned the rotamer most frequently found in protein structures, with the oxygen *cis* to C4 ($\theta_N \sim 180°$). At pH 7.25, the NH_2 of nicotinamide can then serve as a hydrogen-bond donor to the carbonyl oxygen of Gln183 (Figure 2), using the orientation of the Gln183 amide that is uniquely defined in the complex with CH_3-H_4folate (see below). However, at pH 6.0, either the Gln183 side chain or the carboxamide must change orientation relative to the positions assigned for the structure at pH 7.25.

CH_3-H_4Folate Conformation and Interactions. The CH_3-H_4folate product bound to MTHFR adopts an L shape, with the pterin ring perpendicular to the plane of the *para*-aminobenzoyl (PABA) group (Figure 3A). The pterin ring is stacked against the isoalloxazine ring of the flavin. However, the pterin and flavin rings are not completely parallel but are instead tilted by the protrusion of the N5−CH_3 substituent. In this complex, the methyl carbon attached to the N5 of CH_3-H_4folate is 3.34 Å from the flavin N5 and positioned to donate a hydride to the oxidized flavin.

Gln183 and Asp120 both provide bidentate interactions with the pterin ring; Gln183 hydrogen bonds to N1 and NH8, and Asp120 hydrogen bonds to N3 and the exo-NH_2 group at position 2 of the pterin (see Scheme 1 for numbering). The PABA ring is surrounded by a hydrophobic quartet of residues, Leu277, Leu212, Phe184, and Phe223, that form a binding pocket (Figure 3). Phe223 moves from its position in the free enzyme, where it occludes the PABA pocket, to provide one wall of this hydrophobic enclosure. The α-carboxyl group of the glutamate tail interacts with Gln219, while the γ-carboxyl group interacts with Arg279 (Figure 3).

L4 and L2 Loops Adopt Alternate Conformations, and the Distribution of These Conformers Can Be Influenced by pH and Ligand Binding. The β−α connecting loops L4 and L2 can adopt "open" or "closed" conformations in which the distances between key residues and the flavin ring vary. The relative stabilities of these conformations depend upon pH and can be altered by binding of substrates or products (Table 2). The roles of rearrangements of loops L2 and L4 in catalysis are considered in more detail in the Discussion.

In the substrate-free enzyme at pH 6.1 (*17*), loop L4 is closed and L2 is open, whereas at pH 7.4, L4 is open and L2 is closed. The distinguishing features of these conformations are depicted in Figure 4. Loop L4 comprises residues 118−131 and includes part of the conserved sequence, ^{116}ALRGD^{120}. Although the loop is disordered beyond residue 123, the initial residues can adopt at least two different conformations with characteristic but different

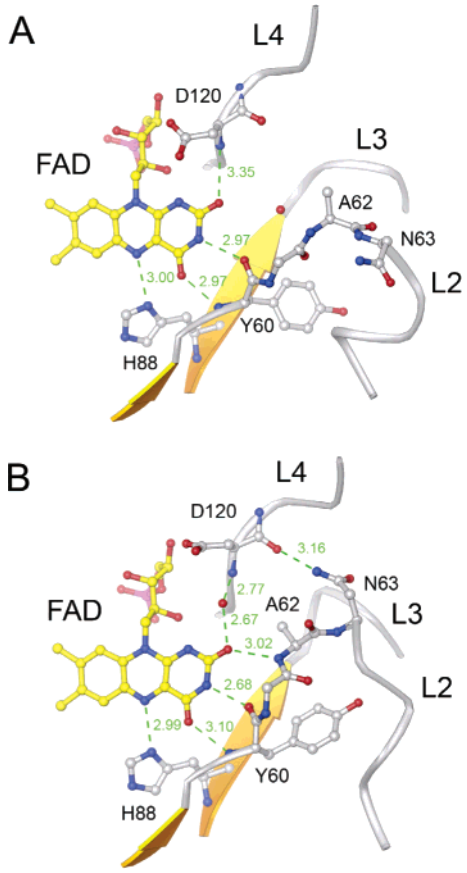

FIGURE 4: pH-dependent changes in the conformations of loops L2, L3, and L4. (A) In the substrate-free enzyme at pH 6.1, L2 is open and L4 is closed. Asp120 is close to the flavin N1 and O2; Ala62 is separated from the flavin, and helix α2 begins at residue 63. (B) In the substrate-free enzyme at pH 7.4, L2 is closed and L4 is open. Asp120 moves away from the flavin, and 62 NH interacts with the flavin O2. Residues 62−65 form a β turn, and helix α2 begins at residue 67. The side chain of Asn63 interacts with loop L4 in its open conformation.

orientations of Asp120. At pH 6.1 (*17*), the Asp120 side chain is positioned close to N1 of the flavin. This "closed" form (Figure 4A) is characterized by a hydrogen bond between NH 120 and the flavin O2 and by a close approach of the carboxylate of Asp120 to the N1−C2=O locus of the flavin. The carboxyl oxygens of Asp120 are 3.78 and 4.71 Å from N1, respectively. In the "open" conformation of L4 observed at pH 7.4, Asp120 forms a different set of hydrogen bonds (Figure 4B). Cα 120 is displaced, and the amide nitrogen of Asp120 moves away from the flavin O2 by more than 1.0 Å relative to its position in the closed conformation. A water molecule bridges O2 and Asp120 NH, and the carboxyl oxygens of Asp120 are approximately 6 Å from the flavin N1.

The open and closed conformations of L2, the connector between β2 and α2, are also illustrated in Figure 4.[2] In the substrate-free enzyme at pH 6.1 (*17*), the L2 loop is a short sequence including only residues 60−62, with Asn63 form-

ing the N-terminal cap of helix α2. This conformation of L2 is "open" in the sense that Ala62 is displaced from the flavin ring, with the flavin O2 and 62 NH separated by about 5 Å (Figure 4A). In contrast, the structure of substrate-free oxidized MTHFR at pH 7.4 reveals a "closed" conformation of L2 with a hydrogen bond between 62 NH and the flavin O2 (Figure 4B). This new hydrogen bond extends the antiparallel arrangement of hydrogen bonds between the pyrimidine portion of the flavin and the backbone segment 60−62. The closed conformation of L2 is achieved by unwinding residues 63−66 of helix α2; residues 61−64 instead form a type-II β turn, and α2 begins at residue 67.

The effects of ligands on the loop conformations are summarized in Table 2. Steric clashes between the Asp120 carboxyl group and the nicotinamide ribose prevent binding of NADH to the closed conformation of loop L4, which must open to allow for formation of the NADH complex at pH 6.0. However, binding of NADH does not induce rearrangement of L2 at either pH 6.0 or 7.25. Similar to the substrate-free enzyme, the L2 loop is open in the NADH complex at pH 6.0 but is closed in the NADH complex at pH 7.25 (Table 2). Binding of CH_3-H_4folate, which hydrogen bonds to Asp120, induces the closure of L4 at pH 7.4 but does not force a rearrangement of L2.

Interactions among Loops L2, L3, and L4. The closed L2 conformation is characterized by a close approach of Ala62 to the flavin. Another key feature of this conformation in substrate-free MTHFR at pH 7.4 is the presence of a hydrogen bond between the side-chain amide of Asn63 and the backbone carbonyl of Asp120, which appears to stabilize the open form of L4 (Figure 4A). Superpositions of the substrate-free structures determined at pH 6.1 and 7.4 reveal that Asn63 in the closed L2 loop overlaps the position of Pro122 in the closed L4 loop. This overlap might have been expected to preclude the simultaneous closing of both L2 and L4. However, in the CH_3-H_4folate complex, movement of Pro122, which can no longer be modeled in the electron density, relieves this potential clash and the L2 and L4 loops are both closed.

The β−α loop L3 (residues 91−95) also undergoes a pH-dependent rearrangement that may be coupled with opening and closing of L2. At pH 6.0, when L2 is open, Arg67 of L2 hydrogen bonds with the carbonyl of Ile92. At higher pH, when L2 is closed, this interaction is broken and replaced by a new hydrogen bond between the hydroxyl of Tyr60 and the carboxylate of Asp93. This rearrangement is accompanied by a peptide flip in L3 at Ile92−Asp93.

DISCUSSION

Pyridine Nucleotide Conformations. Solution NMR studies have previously established the existence of folded pyridine nucleotides in solution (*34*−*36*). Free NAD^+ is an equilibrium mixture of folded and extended molecules. Until recently, only extended pyridine nucleotides had been observed or modeled in protein structures, but there are now three examples of tightly folded pyridine nucleotides bound to flavoenzymes, including the MTHFR−NADH complex. The first observation of a bound NAD^+ hairpin was made by Tanner et al. in their analysis of flavin reductase P (FRP), a flavoprotein that generates free reduced FMN as a substrate for other enzymes, including luciferase (*37*). In the FRP−NAD^+ complex, NAD^+ is an inhibitor and binds the enzyme in a nonproductive fashion, with the pyrophosphate moiety contacting the isoalloxazine ring of the flavin prosthetic group. A productively bound folded NAD^+ was subsequently observed in another flavin reductase, PheA2 (*33*), where the nicotinamide and flavin rings are stacked in an orientation that appears to allow hydride transfer from the nicotinamide C4 to the flavin N5. The binding mode observed in MTHFR similarly displays good geometry for hydride transfer and is presumed to be catalytically competent. NADH can reduce the flavin cofactor when added to crystals of either MTHFR or PheA2 (*33*).

The pyridine nucleotide conformations are almost identical in the productive complexes that are observed in MTHFR and PheA2. Except for small differences at the nicotinamide ribose and phosphate, the hairpins can readily be superimposed. Instead, it is the face of the flavin ring that distinguishes the structures of these two complexes. The *re* side of the isoalloxazine ring stacks against nicotinamide in PheA2, whereas the *si* side is exposed for stacking in MTHFR.

In contrast, there are major differences between the folded form of the pyridine nucleotide in MTHFR and the hairpin that forms an unproductive complex with FRP. The *pro-S* face of nicotinamide is presented to the outside of the hairpin in MTHFR, and the *pro-R* face is buried, whereas in FRP, the *pro-R* face is accessible. Presentation of the *pro-R* face is accomplished by exchanging the positions of the adenine and nicotinamide rings rather than by rotation about the glycosidic N−C1′ bond; the bases are *anti* in both conformations. Interconversion of the hairpins requires large changes in the torsion angles along the C5−O−P−O−P−O−C5 backbone of the dinucleotide. It remains to be seen whether the *pro-R* hydrogen of an NADH conformer like that bound to FRP can be transferred to a flavin cofactor. While the stereospecificity of hydride transfer is usually determined by interactions with the carboxamide group of NAD(H), the entire molecule may be involved in the selection process when NAD(H) is tightly folded.

The most important aspect of NADH binding in *E. coli* MTHFR is the use of stacking and hydrophobic interactions. The stacked NADH hairpin is wedged between Phe223 and the isoalloxazine ring of FAD. It has relatively few hydrogen-bonding interactions with protein residues compared to the interactions commonly observed for extended pyridine nucleotide complexes. The only direct hydrogen bonds are with the invariant Gln183 and Thr59. Despite the limited protein−NADH contacts, the inhibition constant for NADH binding to reduced MTHFR is approximately10 μM and K_d for NADH binding to the oxidized enzyme is 32 μM (*11*). Thus, the stacking and hydrophobic interactions that position the substrate must make significant contributions to the binding energy.

Pyridine Nucleotide Selectivity in MTHFR. Bacterial MTHFRs are selective for NADH, while the mammalian

[2] In the C chains of the new structures reported in this paper, the L2 loop adopts an alternative open conformation with 62 NH displaced from the flavin ring and a partly unraveled α2 helix. The "C-chain" conformation of L2 is a variant that seems to be maintained by intermolecular contacts at the crystallographic 2-fold axis and is not influenced by a shift in pH from 6.1 to 7.4 or by the presence of substrates.

enzymes use NADPH (*4*, *5*). The mode of NADH binding in *E. coli* MTHFR suggests that discrimination against NADPH binding arises from both steric overlap and the absence of strong favorable charge interactions. A model of NADPH based on the known binding mode of NADH places the 2′ phosphate close to Phe30, Leu277, and Glu28 and displaces two solvent molecules. The phosphate is a tight fit but can be modeled without any nonbonded contacts shorter than approximately 3.0 Å. Arg33 and Lys222 are nearby and could exert long-range electrostatic effects, but there are no basic residues to interact directly with the added charge of the 2′ phosphate as is typically the case in enzymes utilizing NADPH (*38*). Therefore, a phosphate at the 2-hydroxyl position may be difficult to accommodate in the active site.

A comparison of the bacterial MTHFR sequences with the sequences of MTHFRs that are specific for NADPH does not show striking differences from the *E. coli* enzyme in any of the residues of the pyridine nucleotide-binding site; in particular, the hydrophobic residues contacting the modeled 2′ phosphate are retained. Thus, although the structure seems to account for the preference of *E. coli* MTHFR for NAD^+/NADH, it does not explain why the mammalian MTHFR enzymes are specific for $NADP^+$/NADPH.

Although Phe223 interacts with each substrate in bacterial MTHFR, stacking with the adenine ring of the pyridine nucleotide during one half-reaction and contacting the PABA moiety in the other, this residue is not invariant. Among 21 bacterial-type (single-domain) MTHFRs displaying sequence identity of 40% or greater with the *E. coli* enzyme (excluding sequences from other *E. coli* strains), Phe is found at this position in 17. Methionine occupies this site in the remaining bacterial sequences. Variations are greater in MTHFRs from higher organisms; Met, Leu, Ile, and Val all occur at the position equivalent to Phe223, but Phe is not observed. Leucine interacts with the adenine ring of the NAD^+ hairpin in the PheA2·NAD^+ complex (*33*).

Binding of Folate and Protonation of N10. The folate half-reaction in MTHFR involves acid-catalyzed ring opening of the five-membered imidazolidine ring of CH_2-H_4folate. Glu28 has been implicated as the general acid that acts by protonating N10 of the folate; its mutation to glutamine renders the enzyme incapable of reducing the CH_2-H_4folate substrate with concomitant oxidation of reduced flavin (*16*). In the structure of the Glu28Gln·CH_3-H_4folate complex, a water bound to Gln28 is located 3.4 Å from N10 of CH_3-H_4folate. A water is observed at the same site in the structure of the substrate-free wild-type enzyme. If Glu28 donates a proton to N10 of the ring-closed substrate via this coordinated water, it can be reprotonated by a relay from the solvent that involves the conserved residues His273 and Ser26. Glu28 is hydrogen-bonded to Nϵ2 of His273, which in turn is hydrogen-bonded to the side chain of Ser26. Ser26 is connected to waters that lead to the bulk solvent. The structure of the CH_3-H_4folate complex therefore supports the conclusion that the Glu28Gln mutation abolishes catalysis of the folate half-reaction by disabling the protonation of N10. In the ternary complex of flavin-independent thymidylate synthase (thyA) with methylenetetrahydrofolate and FdUMP (*39*), a water molecule coordinated by Glu58 is within hydrogen-bonding distance of N10 of folate and has been proposed to play an analogous role (*40*).

The Glu28Gln·CH_3-H_4folate product complex reveals how the enzyme is able to bind folate and position the N5−CH_3 group of folate close to the flavin N5. However, the CH_2-H_4folate substrate cannot be accommodated by the enzyme in the same way as the product CH_3-H_4folate because of the torsional restraints introduced by its closed five-membered imidazolidine ring. It is likely that a conformational change in the substrate accompanies ring opening, allowing the intermediate iminium cation to adopt a binding mode more like that of the product. Attempts to cocrystallize oxidized Glu28Gln MTHFR with CH_2-H_4folate or to diffuse this substrate into preformed crystals have failed to yield images of a bound folate. Docking a model of CH_2-H_4folate, using the folded ring-closed conformation proposed for the ternary complex of thymidylate synthase (*39*), suggests that the PABA ring of CH_2-H_4folate may not be situated in the hydrophobic pocket in the initial complex with MTHFR. The affinity of the PABA pocket for the PABA group may promote the otherwise unfavorable ring opening by stabilizing the iminium cation intermediate. A PABA pocket is observed in both MTHFR and the classical flavin-independent thymidylate synthase (*41*), enzymes that catalyze the opening of the imidazolidine ring of CH_2-H_4folate, but is not found in CH_3-H_4folate methyltransferases (MetE/MetH) (*42*, *43*), suggesting that this feature may be important for catalysis.

Properties and Role of Asp120. It was surprising to find the acidic residue, Asp120, near N1 of the flavin. Flavoproteins more frequently incorporate a basic residue or the N-terminal turn of an α helix at this site; either of these neighbors offers charge compensation for an anionic reduced flavin (*44*, *45*). Aspartate at this position was expected to lower the redox potential of the flavin and to destabilize the anionic hydroquinone species because of unfavorable charge−charge repulsion. A shift in potential was indeed observed in the Asp120Asn mutant, but the change was not dramatic (*16*). Our observation that Asp120 can adopt an open conformation in which the carboxylate group is farther from N1 helps to rationalize the relatively small effect of the Asp120Asn mutation on the potentials of the substrate-free protein.

Asp120 has been proposed to play significant roles in catalysis and in substrate binding during the oxidative half-reaction with methylenetetrahydrofolate (*16*). The Asp120Asn enzyme exhibits a 150-fold decrease in the rate of reduction of CH_2-H_4folate (*16*), suggesting that the charge on Asp120 may stabilize the putative 5-iminium cation intermediate (Scheme 1). The structure of the CH_3-H_4folate complex with the Glu28Gln mutant shows Asp120 in the closed conformation where it forms hydrogen bonds with the 3 NH and the 2-exoNH_2 groups of the product. It is tempting to assign a catalytic role to the closure of loop L4 that brings Asp120 closer to the intermediate cation. Although the Asp120Asn mutation increases the K_d for CH_2-H_4folate by a factor of only 2, recent studies of additional mutants indicate that hydrogen bonding to Asp120 makes significant contributions to the affinity of MTHFR for CH_2-H_4folate (*46*).

Coupling of Loop Conformational Changes and Ligand Binding. The observed variations in the conformations of loops L2 and L4, the partial disordering of L4, and the elevated temperature factors in these loops all indicate that they are mobile regions of the structure and suggest facile

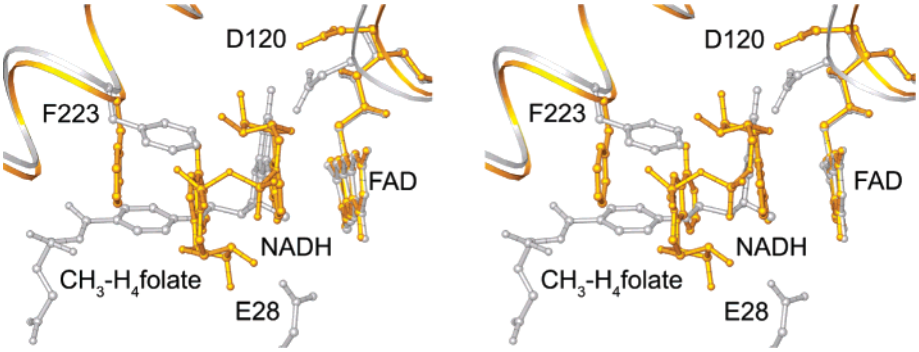

FIGURE 5: Stereoview of the superposition of the MTHFR·NADH complex (gold) and the MTHFR·CH_3-H_4folate complex (gray). The L4 loop and Asp120 move as a rigid unit, with Gly119 providing a hinge. The N5-methyl of CH_3-H_4folate and C4-H of NADH are oriented for hydride transfer to N5 of FAD.

interconversion among the conformations. The groups responsible for triggering the pH-dependent changes have not been identified, but we might expect ligand binding to affect the equilibria near the approximate midpoint of the pH-dependent transitions in the structure. Indeed, binding of NADH at pH 6.0 induces changes in L4. Likewise, formation of the CH_3-H_4folate complex at pH 7.4 is accompanied by closure of L4 and some disordering of the residues downstream of Asp120, changes which probably decrease the measured affinity of MTHFR for the product. The folate complex is the only one of the observed structures in which both L2 and L4 adopt closed conformations.

In free oxidized enzyme at pH 7.4, L2 is closed, whereas L4 is open. We surmise that a structure with L2 closed and L4 open is also preferred by the substrate-free reduced enzyme. This arrangement of the loops lessens charge repulsion by moving Asp120 away from flavin N1 while providing a backbone hydrogen bond to O2, which carries more negative charge in reduced than in oxidized flavins (*45*). Thus, binding of NADH at pH 7.25, observed in the complex of NADH with reduced enzyme, does not appear to require rearrangements of either L2 or L4; L4 must remain open to bind NADH, and L2 remains closed in the complex with NADH.

Ping-Pong Strategy in MTHFR. Many enzymes that catalyze NAD(P)-dependent reactions incorporate a separate domain, often a Rossmann fold, for binding the nucleotide. Among those enzymes that employ flavins as intermediate redox carriers, several strategies have evolved to allow for each of the substrates to access the flavin. In glutathione reductase, the pyridine nucleotide and glutathione disulfide substrates bind at opposite faces of the flavin (*47*); in thioredoxin reductase from *E. coli*, large domain rotations are employed to present first the NADPH and then an enzyme disulfide to the same face of the flavin ring (*48*, *49*). In MTHFR, there is no separate domain for NADH and the same active-site landscape is used to recognize both substrates. A superposition of the structures of the NADH and folate complexes of MTHFR (Figure 5) reveals that the binding sites of the pterin and nicotinamide rings overlap and that Asp120, Gln183, and Phe223 interact with both substrates. However, the AMP moiety of NADH cannot be accommodated in the groove in the enzyme that seems to have been designed for folates.

Thus, bacterial MTHFR has adopted a very simple ping-pong strategy. Binding the pyridine nucleotide as a compact hairpin minimizes the area required for recognition of the reducing substrate and allows the same subset of active-site residues to determine the binding of the two chemically different substrates. Local conformational changes are employed for differential recognition of NADH and tetrahydrofolate. Phe223 stacks tightly against the adenine ring in the NADH complex but swings out to lie over the PABA moiety of tetrahydrofolate. At the opposite end of the active site (Figure 5), loop L4 closes to allow Asp120 to interact with folates but moves away to avoid interference with the binding of the pyridine nucleotide substrate. This Spartan strategy for substrate binding is not nearly as costly as acquiring an additional domain to recognize an extended pyridine nucleotide.

ACKNOWLEDGMENT

The authors dedicate this paper to the late Professor Vincent Massey. They thank Dr. Rowena G. Matthews and Dr. David P. Ballou for critical comments and discussions of the structure and activity of MTHFR and the staff at the DuPont−Northwestern−Dow Collaborative Access Team (DND-CAT) at APS for assistance in collection of the X-ray data. Use of the APS was supported by the U.S. Department of Energy, Basic Energy Sciences, and DND-CAT. Portions of this work were performed at DND-CAT Synchrotron Research Center located at Sector 5 of APS. DND-CAT is supported by the E.I. DuPont de Nemours and Co., the Dow Chemical Co., the U.S. National Science Foundation, and the State of Illinois.

SUPPORTING INFORMATION AVAILABLE

Two orientations of bound NADH (Supplemental Figure 1). This material is available free of charge via the Internet at http://pubs.acs.org.

REFERENCES

1. Delk, A. S., Nagle, D. P., and Rabinowitz, J. C. (1980) Methylenetetrahydrofolate-dependent biosynthesis of ribothymidine in transfer RNA of *Streptococcus faecalis*. Evidence for reduction of the 1-carbon unit by $FADH_2$, *J. Biol. Chem. 255*, 4387−4390.
2. Goyette, P., Sumner, J. S., Milos, R., Duncan, A. M., Rosenblatt, D. S., Matthews, R. G., and Rozen, R. (1994) Human methylenetetrahydrofolate reductase: Isolation of cDNA, mapping and mutation identification [published erratum appears in *Nat. Genet.* (1994) Aug, *7* (4), 551], *Nat. Genet. 7*, 195−200.
3. Sumner, J., Jencks, D. A., Khani, S., and Matthews, R. G. (1986) Photoaffinity labeling of methylenetetrahydrofolate reductase with 8-azidoadenosylmethionine, *J. Biol. Chem. 261*, 7697−7700.

4. Kutzbach, C., and Stokstad, E. L. R. (1971) Mammalian methylenetetrahydrofolate reductase: Partial purification, properties, and inhibition by *S*-adenosylmethionine, *Biochim. Biophys. Acta 250*, 459−477.
5. Sheppard, C. A., Trimmer, E. E., and Matthews, R. G. (1999) Purification and properties of NADH-dependent 5,10-methylenetetrahydrofolate reductase (MetF) from *Escherichia coli*, *J. Bacteriol. 181*, 718−725.
6. Sheppard, C. A., Sumner, J. S., Goyette, P., Frosst, P., Rozen, R., and Matthews, R. G. (1997) Methylenetetrahydrofolate reductase: Comparison of the enzyme from mammalian and bacterial sources, in *Homocysteine Metabolism: From Basic Science to Clinical Medicine* (Graham, I., Refsum, H., Rosenberg, I. H., and Ueland, P. M., Eds.) pp 31−35, Kluwer, Norwell, MA.
7. Saint-Girons, I., Duchange, N., Zakin, M. M., Park, I., Margarita, D., Ferrara, P., and Cohen, G. N. (1983) Nucleotide sequence of *metF*, the *E. coli* structural gene for 5,10-methylenetetrahydrofolate reductase and of its control region, *Nucleic Acids Res. 11*, 6723−6732.
8. Cathou, R. E., and Buchanan, J. M. (1963) Enzymatic synthesis of the methyl group of methionine. V. Studies with 5,10-methylenetetrahydrofolate reductase from *Escherichia coli*, *J. Biol. Chem. 238*, 1746−1751.
9. Katzen, H. M., and Buchanan, J. M. (1965) Enzymatic synthesis of the methyl group of methionine. VIII. Repression-derepression, purification, and properties of 5,10-methylenetetrahydrofolate reductase from *Escherichia coli*, *J. Biol. Chem. 240*, 825−835.
10. Daubner, S. C., and Matthews, R. G. (1982) Purification and properties of methylenetetrahydrofolate reductase from pig liver, in *Flavins and Flavoproteins* (Massey, V., and Williams, C. H., Eds.) pp 165−172, Elsevier, New York.
11. Trimmer, E. E., Ballou, D. P., and Matthews, R. G. (2001) Methylenetetrahydrofolate reductase from *Escherichia coli*: Elucidation of the kinetic mechanism by steady-state and rapid-reaction studies, *Biochemistry 40*, 6205−6215.
12. Vanoni, M. A., Ballou, D. P., and Matthews, R. G. (1983) Methylenetetrahydrofolate reductase: Steady state and rapid reaction studies on the NADPH−methylenetetrahydrofolate, NADPH−menadione, and methyltetrahydrofolate−menadione oxidoreductase activities of the enzyme, *J. Biol. Chem. 258*, 11510−11514.
13. Vanoni, M. A., and Matthews, R. G. (1984) Kinetic isotope effects on the oxidation of NADPH by the flavoprotein methylenetetrahydrofolate reductase, *Biochemistry 23*, 5272−5279.
14. Sumner, J. S., and Matthews, R. G. (1992) Stereochemistry and mechanism of hydrogen transfer between NADPH and methylenetetrahydrofolate in the reaction catalyzed by methylenetetrahydrofolate reductase from pig liver, *J. Am. Chem. Soc. 114*, 6949−6956.
15. Lee, Y. H., Nadaraia, S., Gu, D., Becker, D. F., and Tanner, J. J. (2003) Structure of the proline dehydrogenase domain of the multifunctional PutA flavoprotein, *Nat. Struct. Biol. 10*, 109−114.
16. Trimmer, E. E., Ballou, D. P., Ludwig, M. L., and Matthews, R. G. (2001) Folate activation and catalysis in methylenetetrahydrofolate reductase from *Escherichia coli*: Roles for aspartate 120 and glutamate 28, *Biochemistry 40*, 6216−6226.
17. Guenther, B. D., Sheppard, C. A., Tran, P., Rozen, R., Matthews, R. G., and Ludwig, M. L. (1999) The structure and properties of methylenetetrahydrofolate reductase from *Escherichia coli* suggest how folate ameliorates human hyperhomocysteinemia, *Nat. Struct. Biol. 6*, 359−365.
18. Otwinowski, Z., and Minor, W. (1997) Processing of X-ray diffraction data collected in the oscillation mode, *Methods Enzymol. 276*, 307−326.
19. Kabsch, W. (1993) Automatic processing of rotation diffraction data from crystals of initially unknown symmetry and cell constants, *J. Appl. Crystallogr. 26*, 795−800.
20. French, S., and Wilson, K. (1978) On the treatment of negative intensity observations, *Acta Crystallogr., Sect. A: Found. Crystallogr.*, 517−525.
21. Vagin, A., and Templyakov, A. (1997) MOLREP: An automated program for molecular replacement, *J. Appl. Crystallogr. 30*, 1022−1025.
22. Kissinger, C. R., Gehlhaar, D. K., and Fogel, D. B. (1999) Rapid automated molecular replacement by evolutionary search, *Acta Crystallogr., Sect. D: Biol. Crystallogr. 55*, 484−491.
23. Brünger, A. T., Adams, P. A., Clore, G. M., DeLano, W. L., Gros, P., Grosse-Kunstleve, R. Q., Jiang, J.-S., Kuszewski, J., Nilges, M., Pannu, N. S., Read, R. J., Rice, L. M., Simonson, T., and Warren, G. L. (1998) Crystallography and NMR system: A new software suite for macromolecular structure determination, *Acta Crystallogr., Sect. D: Biol. Crystallogr. 54*, 905−921.
24. Sheldrick, G. M., and Schneider, T. R. (1997) SHELXL: High-resolution refinement, *Methods Enzymol. 277*, 319−343.
25. McRee, D. E. (1999) XtalView/Xfit−A versatile program for manipulating atomic coordinates and electron density, *J. Struct. Biol. 125*, 156−165.
26. van Aalten, D. M. F., Bywater, R., Findlay, J. B. C., Hendlich, M., Hooft, R. W. W., and Vriend, G. (1996) PRODRG, a program for generating molecular topologies and unique molecular descriptors from coordinates of small molecules, *J. Comput.-Aided Mol. Des. 10*, 255−262.
27. Laskowski, R. A., MacArthur, M. W., Moss, D. S., and Thornton, J. M. (1993) PROCHECK: A program to check the stereochemical quality of protein structures, *J. Appl. Crystallogr. 26*, 283−291.
28. Vaguine, A. A., Richelle, J., and Wodak, S. J. (1999) SFCHECK: A unified set of procedures for evaluating the quality of macromolecular structure-factor data and their agreement with the atomic model, *Acta Crystallogr., Sect. D: Biol. Crystallogr. 55*, 191−205.
29. Bell, C. E., Yeates, T. O., and Eisenberg, D. (1997) Unusual conformation of nicotinamide adenine dinucleotide (NAD) bound to diphtheria toxin: A comparison with NAD bound to oxidoreductase enzymes, *Protein Sci. 6*, 2084−2096.
30. Moodie, S. L., and Thornton, J. M. (1993) A study into the effects of protein binding on nucleotide conformation, *Nucleic Acids Res. 21*, 1369−1380.
31. Deng, Z., Aliverti, A., Zanetti, G., Arakaki, A. K., Ottado, J., Orellano, E. G., Calcaterra, N. B., Ceccarelli, E. A., Carillo, N., and Karplus, P. A. (1999) A productive $NADP^+$ binding mode of ferredoxin-$NADP^+$ reductase revealed by protein engineering and crystallographic studies, *Nat. Struct. Biol. 6*, 847−853.
32. Torres, R., Schiott, B., and Bruice, T. C. (1999) Molecular dynamics simulations of ground and transition states for the hydride transfer from formate to NAD^+ in the active site of formate dehydrogenase, *J. Am. Chem. Soc. 121*, 8164−8170.
33. van den Heuvel, R. H. H., Westphal, A. H., Heck, A. J. R., Walsh, M. A., Rovida, S., van Berkel, W. J. H., and Mattevi, A. (2004) Structural studies on flavin reductase PheA2 reveal binding of NAD in an unusual folded conformation and support novel mechanism of action, *J. Biol. Chem. 279*, 12860−12867.
34. Hull, R. V., Conger, P. S., III, and Hoobler, R. J. (2001) Conformation of NADH studied by fluorescence excitation spectroscopy, *Biophys. Chem. 90*, 9−16.
35. Jardetzky, O., and Wade-Jardetzky, N. G. (1966) The conformation of pyridine dinucleotides in solution, *J. Biol. Chem. 241*, 85−91.
36. Smith, P. E., and Tanner, J. J. (2000) Conformations of nicotinamide adenine dinucleotide (NAD^+) in various environments, *J. Mol. Recognit. 1*, 27−34.
37. Tanner, J. J., Tu, S.-C., Barbour, L. J., Barnes, C. L., and Krause, K. L. (1999) Unusual folded conformation of nicotinamide adenine dinucleotide bound to flavin reductase P, *Protein Sci. 8*, 1725−1732.
38. Ratnam, K., Ma, H., and Penning, T. M. (1999) The arginine 276 anchor for NADP(H) dictates fluorescence kinetic transients in 3 α-hydroxysteroid dehydrogenase, a representative aldo-keto reductase, *Biochemistry 38*, 7856−7864.
39. Hyatt, D. C., Maley, F., and Montfort, W. R. (1997) Use of strain in a stereospecific catalytic mechanism: Crystal structures of *Escherichia coli* thymidylate synthase bound to FdUMP and methylenetetrahydrofolate, *Biochemistry 36*, 4585−4594.
40. Zapf, J. W., Weir, M. S., Emerick, V., Villafranca, J. E., and Dunlap, R. B. (1993) Substitution of glutamine for glutamic acid-58 in *Escherichia coli* thymidylate synthase results in pronounce decreases in catalytic activity and ligand binding, *Biochemistry 32*, 9274−9281.
41. Finer-Moore, J. S., Santi, D. V., and Stroud, R. M. (2003) Lessons and conclusions from dissecting the mechanism of a bisubstrate enzyme: Thymidylate synthase mutagenesis, function, and structure, *Biochemistry 42*, 248−256.
42. Evans, J. C., Huddler, D. P., Hilgers, M. T., Romanchuk, G., Matthews, R. G., and Ludwig, M. L. (2004) Structures of the N-terminal modules imply large domain motions during catalysis by methionine synthase, *Proc. Natl. Acad. Sci. U.S.A. 101*, 3729−3736.

43. Pejchal, R., and Ludwig, M. L. (2005) Cobalamin-independent methionine synthase (MetE): A face-to-face double barrel that evolved by gene duplication, *PLoS Biol. 3*, 254−265.
44. Fraaije, M. W., and Mattevi, A. (2000) Flavoenzymes: Diverse catalysts with recurrent features, *Trends Biochem. Sci. 25*, 126−132.
45. Massey, V. (1995) Introduction: Flavoprotein structure and mechanism, *FASEB J. 9*, 473−475.
46. Trimmer, E. E., Ballou, D. P., Galloway, L. J., Scannell, S. A., Brinker, D. R., and Casas, K. R. (2005) Aspartate 120 of *Escherichia coli* methylenetetrahydrofolate reductase: Evidence for major role in folate binding and catalysis, minor role in flavin reactivity, *Biochemistry 44*, 6809−6822.
47. Karplus, P. A., and Schulz, G. E. (1987) Refined structure of glutathione reductase at 1.54 Å resolution, *J. Mol. Biol. 195*, 701−729.
48. Waksman, G., Krishna, T. S., Williams, C. H., Jr., and Kuriyan, J. (1994) Crystal structure of *Escherichia coli* thioredoxin reductase refined at 2 Å resolution. Implications for a large conformational change during catalysis, *J. Mol. Biol. 236*, 800−816.
49. Lennon, B. W., Williams, C. H., Jr., and Ludwig, M. L. (2000) Twists in catalysis: Alternating conformations of thioredoxin reductase from *Escherichia coli*, *Science 289*, 1190−1194.

BI050533Q